

# RESEARCH ARTICLE

OPEN 3 ACCESS

# A height-dependent climatological model of the equatorial ionospheric zonal plasma drifts (EZDrifts): Description and application to an analysis of the longitudinal variations of the zonal drifts

Alexander A. Massoud<sup>1,\*</sup>, Sam A. Shidler<sup>2</sup>, and Fabiano S. Rodrigues<sup>1</sup>

Received 15 September 2022 / Accepted 1 March 2023

Abstract - We introduce the implementation of a global climatological model of the equatorial ionospheric F-region zonal drifts (EZDrifts) that is made available to the public. The model uses the analytic description of the zonal plasma drifts presented by Haerendel et al. (1992) [J Geophys Res 97(A2): 1209–1223] and is driven by climatological models of the ionosphere and thermosphere under a realistic geomagnetic field configuration. EZDrifts is an expansion of the model of the zonal drifts first presented by Shidler & Rodrigues (2021) [Prog Earth Planet Sci 8: 26] which was only valid for the Jicamarca longitude sector and two specific solar flux conditions. EZDrifts now uses vertical equatorial plasma drifts from Scherliess & Fejer (1999) [J Geophys Res 104(A4): 6829–6842] model which allows it to provide zonal drifts for any day of the year, longitude, and solar flux condition. We show that the model can reproduce the main results of the Shidler & Rodrigues (2021) [Prog Earth Planet Sci 8: 26] model for the Peruvian sector. We also illustrate an application of EZDrifts by presenting and discussing longitudinal variabilities produced by the model. We show that the model predicts longitudinal variations in the reversal times of the drifts that are in good agreement with observations made by C/NOFS. EZDrifts also predicts longitudinal variations in the magnitude of the drifts that can be identified in the June solstice observations made by C/NOFS. We also point out data-model differences observed during Equinox and December solstice. Finally, we explain that the longitudinal variations in the zonal plasma drifts are caused by longitudinal variations in the latitude of the magnetic equator and, consequently, in the wind dynamo contributing to the resulting drifts. EZDrifts is distributed to the community through a public repository and can be used in applications requiring an estimate of the overall behavior of the equatorial zonal drifts.

Keywords: Ionosphere / equatorial / electric fields / drifts / zonal

## 1 Introduction

Ionospheric  $\mathbf{E} \times \mathbf{B}$  plasma drifts in the magnetic equatorial F-region are observable manifestations of complex current systems at low and mid-latitudes (Eccles, 2004; Alken et al., 2011). These drifts are also responsible for the dynamics of the ionospheric plasma at equatorial, low, and mid-latitudes with implications in fundamental and applied studies of the Earth's geospace.

The vertical component of the  $\mathbf{E} \times \mathbf{B}$  equatorial plasma drifts has received substantial attention. This is, for the most part, because they contribute to the latitudinal distribution of

the ionospheric plasma at low latitudes through the fountain effect that creates the equatorial ionization anomaly – EIA (Klobuchar et al., 1991). Additionally, the magnitude of the vertical drifts in the evening sector is known to be related to the development of post-sunset equatorial spread F – ESF (Fejer et al., 1999; Smith et al., 2016). This has motivated various experimental and theoretical studies of vertical drifts, including the development of a climatological global model of vertical drifts (Scherliess & Fejer, 1999). This drift model is commonly used to drive numerical models of the ionosphere (Zhan & Rodrigues, 2018; Smith & Klenzing, 2022), to evaluate plasma drift measurements (Stoneback et al., 2011; Rodrigues et al., 2013), and to assess the results of simulations of the ionospheric electrodynamics (Liu et al., 2018; Shidler & Rodrigues, 2022).

<sup>&</sup>lt;sup>1</sup> The University of Texas at Dallas, Richardson, TX 75080, USA

<sup>&</sup>lt;sup>2</sup> Applied Research Laboratories, University of Texas at Austin, Austin, TX 78758, USA

<sup>\*</sup>Corresponding author: Alexander. Massoud@utdallas.edu

The zonal component of equatorial  $\mathbf{E} \times \mathbf{B}$  plasma drifts is also important from both fundamental as well as applied perspectives. Under certain conditions, zonal drifts can also serve as indicators of the dynamics of the thermospheric neutral wind behavior (Coley & Heelis, 1989). It has also been brought to attention that the vertical shear in the evening zonal plasma drifts can be associated with the development of plasma instabilities and ESF formation (Hysell & Kudeki, 2004; Kudeki et al., 2007). Additionally, the behavior of the background plasma drifts seems to be closely related to the zonal motion of large-scale ESF plasma depletions (Chapagain et al., 2013). Therefore, equatorial zonal plasma drifts are intimately related to space weather conditions at low latitudes.

In a recent effort, Shidler & Rodrigues (2021) used long-term Jicamarca incoherent scatter radar (ISR) measurements of vertical and zonal F-region plasma drifts and climatological models of the ionosphere and thermosphere system to create a climatological model of height-dependent quiet-time zonal plasma drifts. They showed that the model was able to reproduce fairly well the mean behavior of the zonal drifts as observed by the Jicamarca ISR. Because the model was driven by height-dependent averages of the vertical drifts only available for the Jicamarca location, three seasons, and two solar flux conditions, the application of the model is somewhat limited. It is particularly useful, however, for cases when self-consistent vertical and zonal components of the equatorial F-region plasma drifts are needed. This could be the case, for instance, when electrodynamic model outputs are being evaluated.

Here, we present an extension of the Shidler & Rodrigues (2021) model referred to as the Equatorial Zonal plasma Drifts (EZDrifts) model. EZDrifts is capable of providing climatological estimates of the quiet-time height-dependent F-region zonal plasma drifts for any day of the year, longitude, and solar flux condition. The climatological model of the equatorial zonal drifts that are currently available (Fejer et al., 2005) takes into consideration geomagnetic activity, but it is height-averaged, and it is only valid for the Jicamarca longitude sector (~76° W). EZDrifts is written in Python for easier use and it is distributed to the public. As an example of the model capabilities, we show that EZDrifts can produce longitudinal variations that have been detected in satellite observations. We also explain the longitudinal variations.

### 2 Methods and analyses

#### 2.1 Analytic model of the zonal plasma drifts

Shidler & Rodrigues (2021), hereinafter referred to as SR21, implemented a simple climatological model describing the morphology of equatorial F-region zonal plasma drifts. The model is based on the work of Haerendel et al. (1992) which showed that a two-dimensional (2D) representation of the low-latitude electrodynamics can describe the height-dependent features of equatorial electric fields including the vertical shear in the zonal plasma drifts associated with equatorial evening vortex (Eccles et al., 1999; Kudeki & Bhattacharyya, 1999; Rodrigues et al., 2012). This 2D representation is derived from integrating the three-dimensional current continuity equation along magnetic field lines. The integration is carried out from the base of the ionosphere, where parallel currents are expected to vanish,

and produces a 2D continuity equation in the magnetic equatorial plane (Eccles et al., 2015):

$$\frac{1}{R_E L} \left( \frac{\partial}{\partial L} (L J_L) + \frac{\partial J_\phi}{\partial \phi} \right) = 0 \tag{1}$$

where  $R_E$  is the radius of the Earth, L is the radial distance in the equatorial plane measured in Earth's radii, and  $\phi$  is the longitude. The integrated vertical current  $(J_L)$ , and the integrated zonal current  $(J_{\phi})$  are defined as (Haerendel et al., 1992):

$$J_L = \Sigma_P \Big( E_L + B U_\phi^P \Big) - \Sigma_H (E_\phi - B U_L^H)$$
 (2)

$$J_{\phi} = \tilde{\Sigma}_{P} \left( E_{\phi} - B U_{L}^{P} \right) + \Sigma_{H} \left( E_{L} + B U_{\phi}^{H} \right)$$
 (3)

where B is the magnitude of the geomagnetic field,  $E_L$  is the vertical electric field,  $E_\phi$  is the zonal electric field,  $\Sigma_P$  and  $\Sigma_H$  are the field-line integrated Pedersen conductivity and Hall conductivity, respectively,  $U_\phi^P$  and  $U_L^P$  represent the field-line averaged zonal and meridional neutral winds weighted by the Pedersen conductivity, respectively, and  $U_\phi^H$  and  $U_L^H$  represents the field-line averaged zonal and meridional neutral winds weighted by the Hall conductivity. The zonal and meridional wind components are with respect to the magnetic field direction and have been properly evaluated in our calculations. The tilde in  $\tilde{\Sigma}_P$  represents the field-line integrated Pedersen conductivity with slightly different geometric factors used in the integration. Further details about the field-line integrated quantities above are provided in Haerendel et al. (1992). Expressions for the collision frequencies used in deriving the Pedersen and Hall conductivities are provided in SP21

Equation (3) can be rearranged to obtain an expression for the vertical electric field  $(E_L)$ :

$$E_{L} = -BU_{\phi}^{P} + \frac{\Sigma_{H}}{\Sigma_{P}}(-BU_{L}^{H} + E_{\phi}) + \frac{J_{L}}{\Sigma_{P}}.$$
 (4)

Dividing equation (4) by -B and substituting the F-region zonal  $(U_i = -E_I/B)$  and vertical  $(W_i = E_\phi/B)$  plasma drifts results in the following expression:

$$U_i = U_\phi^P + \frac{\Sigma_H}{\Sigma_P} U_L^H - \frac{\Sigma_H}{\Sigma_P} W_i - \frac{J_L}{B\Sigma_P}.$$
 (5)

SR21 used equation (5) to create a simple data-aided model capable of describing the height-versus-local time variation of the zonal plasma drifts in the equatorial F-region ionosphere.

In their model, the thermospheric and ionospheric parameters used to compute the field-line integrated variables on the right-hand side of equation (5) are obtained from widely used empirical models. Geomagnetic field values and the coordinates of the geomagnetic dip equator are determined from the International Geomagnetic Field (IGRF-12) model (Thébault et al., 2015). Neutral densities and temperatures are derived from NRL's Mass Spectrometer and Incoherent Scatter (NRLMSISE-00) model (Picone et al., 2002). Ionospheric densities and temperatures are derived from the International Reference Ionosphere (IRI-2016) model (Bilitza et al., 2017). Following the model of SR21, neutral winds for EZDrifts can be determined from the three different versions of the

Horizontal Wind Model (HWM93, HWM07, and HWM14) (Hedin et al., 1996; Drob et al., 2008, 2015). In the example analyses reported here, we use neutral winds provided by the latest model, HMW14. Here, we must remind the reader that only HWM93 has solar flux dependence, and it can be selected as the driver in studies requiring an analysis of the solar flux effects on the zonal plasma drifts. Examples of the results of using HWM93, HWM07, and HMW14 for different solar flux conditions are presented and discussed by SR21. Finally, the height-versus-local time variation of the vertical plasma drifts  $(W_i)$  comes from long-time measurements made by the Jicamarca incoherent scatter radar (ISR). Average drifts were derived for three seasons and two distinct solar flux conditions. Similar to previous studies (Eccles, 1998; Chau & Woodman, 2004; Rodrigues et al., 2012; Hui & Fejer, 2015; Richmond et al., 2015; Shidler & Rodrigues, 2021) which describe the lack of information about  $J_L$  and expectations of a small contribution from  $J_L$  to the total zonal drifts, the last term in equation (5) is neglected in this modeling effort.

#### 2.2 EZDrifts

The SR21 model is capable of reproducing most of the features in the zonal plasma drifts observed by the Jicamarca ISR. More importantly, it allows us to evaluate the impact of different drivers on the morphology of the zonal drifts. The SR21 model, however, is limited to average vertical drift inputs determined from Jicamarca ISR long-term measurements. As a result, the model is limited to the Jicamarca longitude sector (~76° W) and only two distinct solar flux conditions.

In order to estimate F-region zonal drifts at other longitude sectors and over a wider range of solar flux conditions we devoted efforts to creating the new global model of the equatorial F-region zonal plasma drifts (EZDrifts) whose results are presented here. EZDrifts replaces the height-dependent (200–600 km) averages of F-region vertical drifts in the SR21 model with the vertical drifts provided by the Scherliess & Fejer (1999) model (SF99), allowing it to provide estimates of the F-region zonal drifts for any longitude sector and solar flux condition.

The SF99 model is a climatological model of the mean F-region vertical drifts and, therefore, does not have a height dependence. Shidler & Rodrigues (2019) and Shidler et al. (2019), however, showed that while significant height variations can be observed in the vertical drift profiles for a given day, particularly near sunrise and sunset, this height variability is not significant when looking at averages or climatologies of the drifts. Therefore, we anticipated that switching the SR21 vertical drifts from Jicamarca with the SF99 drifts would have minimal effects on the estimated morphology of the drifts. Among other things, this report will describe the results of our analyses that confirm that the SF99 model can indeed be used as a driver.

In addition to using SF99 drifts, EZDrifts also includes a small modification related to IRI inputs. More specifically, EZDrifts requires user-specified values for the Rz12 and IG12 indices. Rz12 is a 13-month running mean of the sunspot number. IG12 is an ionospheric index based on foF2 measurements from a dozen ionosondes correlated with the CCIR foF2. The use of these indices allows for better specification of F-region electron densities by IRI (Bilitza, 2018).

### 3 Results and discussion

We now present examples that illustrate EZDrifts outputs. We start by showing that EZDrifts is capable of reproducing the results of SR21 for the Jicamarca longitude sector. Then, we present EZDrifts predictions of the longitudinal variability of the zonal drifts for different seasons and different heights. The presentation of model results is followed by a comparison with observations made by the C/NOFS satellite. Main similarities and differences are highlighted and discussed. Finally, we analyze the drivers of the zonal plasma drift morphology and explain the effect of the longitudinal variation of the Earth's magnetic field on the longitudinal variation of the zonal drifts predicted by EZDrifts.

# 3.1 On the use of SF99 vertical drifts to estimate zonal drifts

To quantify the effect of replacing the height-dependent average vertical drifts used by SR21 with the height-independent SF99 vertical drifts on the modeled morphology of the zonal drifts, we compared the zonal drifts predicted by the SR21 model with the zonal drifts obtained by EZDrifts for the longitude sector of the Jicamarca Radio Observatory (JRO). The comparison is summarized in Figure 1.

The left column panels of Figure 1 show SR21 results for seasons and solar flux conditions under which the model is valid. The black areas are caused by the lack of vertical drift observations at those altitudes and local times which drive the model. It can be seen that these areas occur at high altitudes during nighttime when ISR echoes are weak and accurate measurements cannot be obtained. These areas also occur in the bottom side F-region after sunset hours where coherent scatter radar echoes often occur and make ISR measurements unreliable. The middle column shows the results obtained with EZDrifts. Because SF99 drifts are used, no gaps (black areas) in the zonal drifts are seen. Finally, the right column shows the difference between the models, that is, SR21–EZDrifts. The results of Figure 1 were obtained using the latest horizontal wind model, HWM14.

As discussed by SR21, the simple analytical model is capable of reproducing the main features of the morphology of the equatorial zonal drifts. For instance, it reproduces the relatively weak westward drifts during daytime and stronger eastward drifts at night that are seen in measurements. It also reproduces the significant height variations in the zonal drifts around sunset hours that are associated with the equatorial plasma vortex (Eccles et al., 1999; Kudeki & Bhattacharyya, 1999; Rodrigues et al., 2012).

As expected, the EZDrifts results in Figure 1 (central column) also reproduce the main features of the zonal drifts. Despite the use of the height-independent SF99 model drifts, EZDrifts produces zonal drifts that resemble those produced by the SR21 model, but without the gaps since vertical drifts are available at all times and heights. To better quantify the agreement between SR21 and EZDrifts, the right-hand side column of Figure 1 shows the differences between the drifts produced by the two models. This comparison shows that differences rarely exceed 4 m/s for all conditions and are, on average,  $\leq 2$  m/s. In general, differences exceeding 4 m/s occur

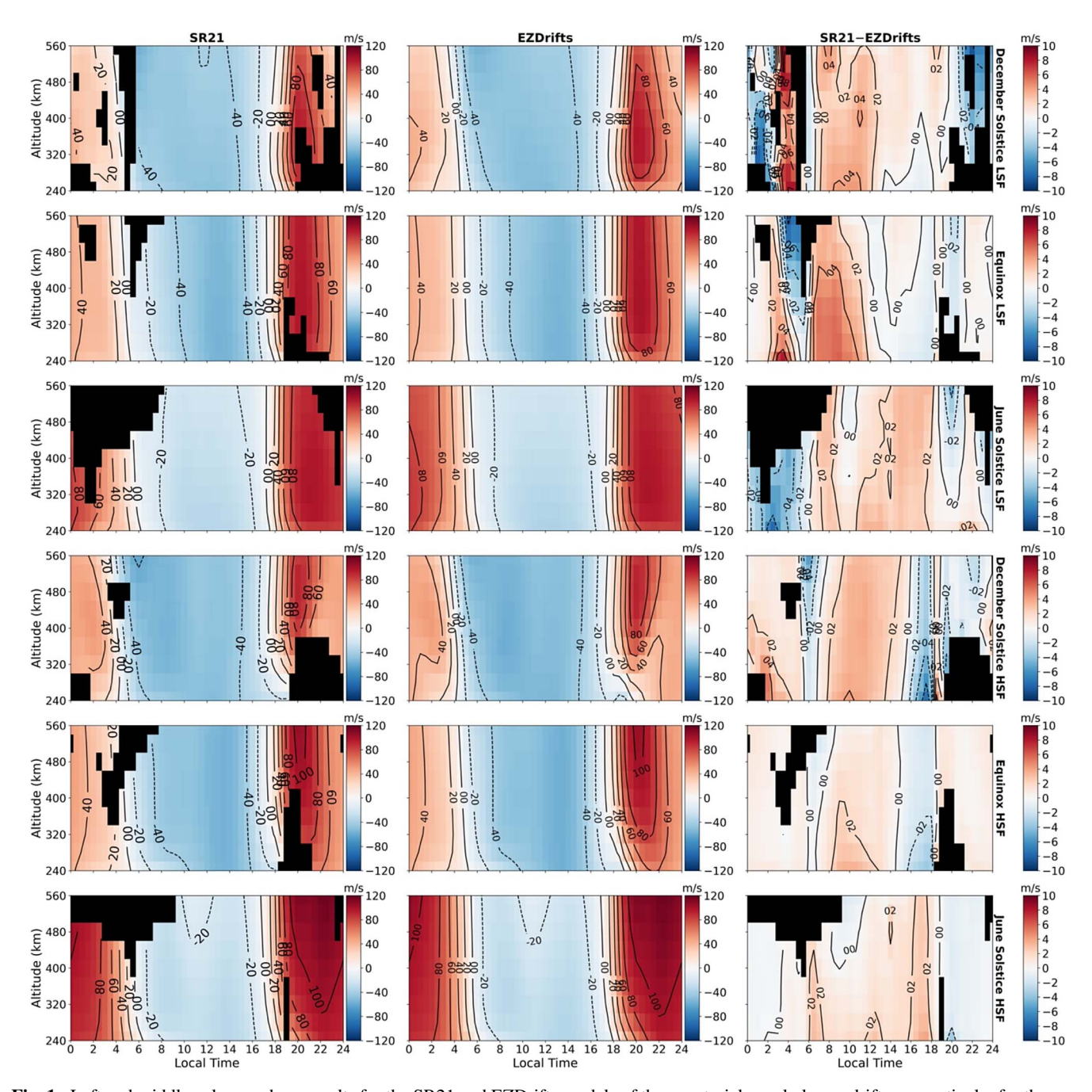


**Fig. 1.** Left and middle columns show results for the SR21 and EZDrifts models of the equatorial zonal plasma drifts, respectively, for the same longitude of Jicamarca Radio Observatory. The right column shows differences between the two model predictions, that is, SR21-EZDrifts. Rows are organized by season and solar flux conditions.

when ionospheric densities and the accuracy of the vertical drift ISR measurements (inputs to SR21) are reduced, that is, during late night/morning hours or topside altitudes. This serves to confirm that using the SF99 model drifts does not cause any significant changes in the predicted zonal drifts with respect to SR21.

## 3.2 Longitudinal variations predicted by EZDrifts

The previous section showed that EZDrifts reproduces the results of SR21. SR21 already presented an extensive comparison of their model results with zonal measurements made by the Jicamarca ISR. In this report, we focus on describing the ability of EZDrifts to produce variations in the zonal drifts as a function of longitude.

We present EZDrifts results in Figure 2 that illustrate the longitudinal variation of the estimated zonal drifts. Figure 2 shows the variation of the equatorial zonal drifts as a function of local time and longitude for three distinct seasons and two different heights. More specifically, Figure 2 shows the drifts in the magnetic zonal direction in the magnetic equatorial plane

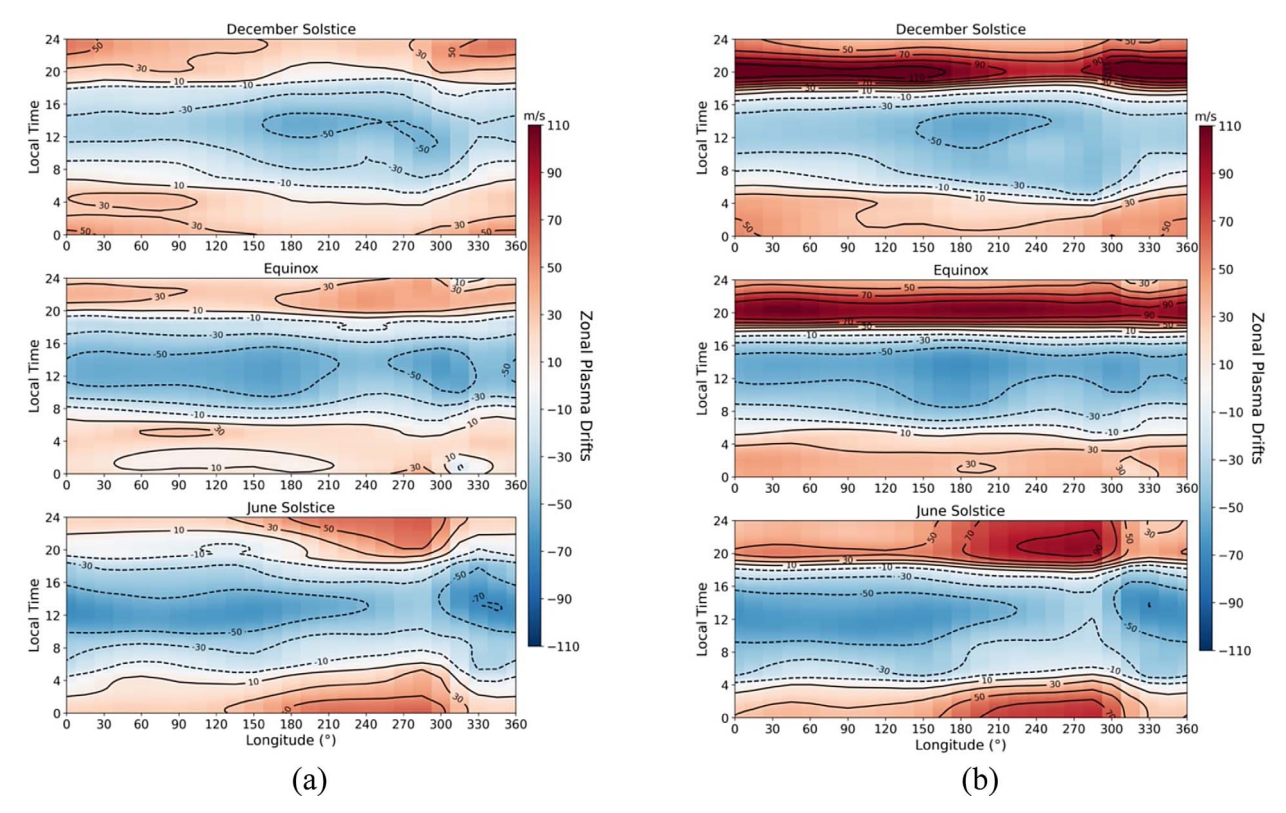


**Fig. 2.** (a) Variations in the quiet-time equatorial zonal drifts (positive eastward) at 200 km produced by EZDrifts as a function of local time, longitude, and season (Dec. 21, Mar. 21, and Jun. 21). (b) Same as (a) but for 400 km altitude. Computations for low solar flux conditions (F10.7 = 73.7 SFU).

for two distinct heights, 200 and 400 km. The calculations are for December solstice (Dec. 21), Equinox (Mar. 21), and June Solstice (Jun. 21). Model results are for low solar flux conditions (F10.7  $\sim$  73.7 SFU) and geomagnetic quiet time (Kp = 1.00, Ap = 4) averaged over when the C/NOFS satellite was making observations of low latitude drifts (within 5° of the magnetic equator). Comparisons with C/NOFS measurements will be presented and discussed in the following sub-section. Figure 2 serves to show that EZDrifts produce equatorial zonal plasma drifts with noticeable height and longitude variations.

The height variations can be seen by comparing the results in Figure 2a (200 km) with the results in Figure 2b (400 km). The height variations are more noticeable in the nighttime drifts, with drifts being stronger at 400 km than at 200 km, particularly in the pre-midnight sector. SR21 already showed that daytime drifts very weakly with height. The height variation in the pre-midnight drifts is the manifestation of a vertical shear in the zonal plasma drifts that have been commonly observed near the magnetic equator and is associated with equatorial plasma vortex (Eccles et al., 1999; Kudeki & Bhattacharyya, 1999; Rodrigues et al., 2012).

In addition to the expected height variation of the zonal drifts, EZDrifts results also show noticeable longitudinal variations. The main longitudinal variations are related to (i) the reversal times of the drifts near sunset and sunrise and (ii) the magnitude of the drifts. The longitudinal variations in the magnitude of the drifts are also more noticeable in the nighttime

drifts. The variations in the reversal times and magnitudes can be seen at both 200 and 400 km altitudes. The variations in the reversal times refer to noticeable changes in the direction of drifts around dawn and dusk that can be seen between about 180° E and 330° E, particularly during June and December solstices. The variations in the reversal times are accompanied by variations in the magnitude of the drifts in the same longitude sector. It can be seen in Figure 2 that the nighttime drifts tend to decrease between 180° E and 330° E during the December solstice. During the June solstice, however, the zonal drifts tend to increase in the same longitude sector.

#### 3.3 Comparison with observations

We now present and discuss a comparison of EZDrifts results with observations. We compare model results with the observed longitudinal variation of the F-region zonal drifts reported by Fejer et al. (2013).

Fejer et al. (2013) analyzed the zonal  $\mathbf{E} \times \mathbf{B}$  drifts measured by the Vector Electric Field Instrument (VEFI) on the Communication/Navigation Outage Forecasting System (C/NOFS) satellite. C/NOFS was launched on April 16, 2008, into a 401  $\times$  867 km orbit with a 13° inclination and orbital period of 97.3 min. The observations analyzed by Fejer et al. (2013) were made between May 2008 and February 2011, a period of very low solar flux conditions (average F10.7 = 73.7 SFU). Only observations made during geomagnetically quiet periods (Kp  $\leq$  3) were considered in their analyses.

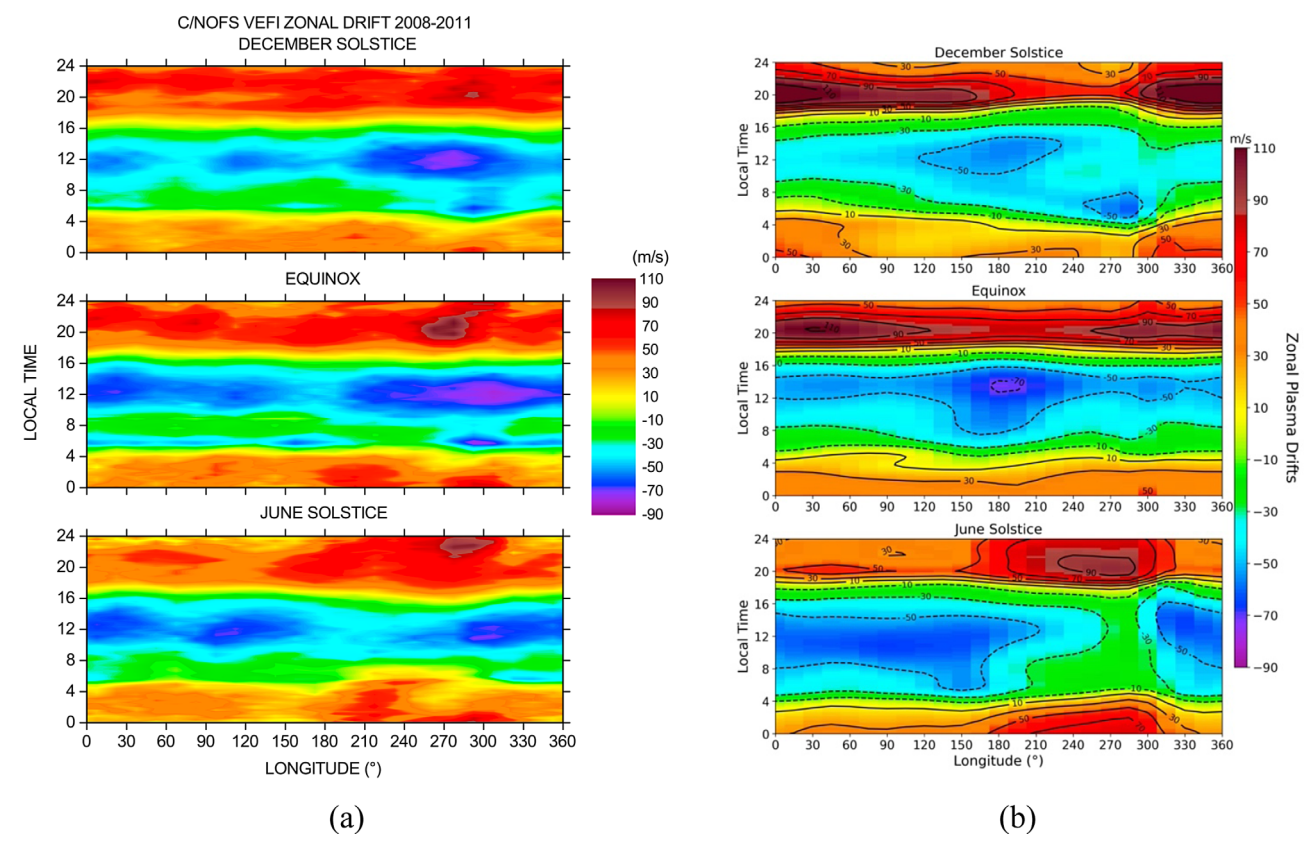


**Fig. 3.** (a) Variations in the quiet-time, LSF equatorial zonal drifts (positive eastward) measured by C/NOFS as a function of local time, longitude, and season. Reproduced from Fejer et al. (2013). Note that the color bar varies from -90 m/s to 110 m/s. (b) Variations in the quiet-time, LSF equatorial zonal drifts (positive eastward) at C/NOFS average height (650 km) produced by EZDrifts as a function of local time, longitude and season (Dec. 21, Mar. 21, and Jun. 21).

For comparison purposes, Figure 3a reproduces the results of Fejer et al. (2013). Similar to Figure 2, their results are organized in three seasons and show the zonal drifts as a function of longitude and local time. Figure 3b shows the zonal drifts predicted by EZDrifts also organized by season. The color map used in Figure 3b accompanied by contours of drift values was chosen to increase the clarity of the overall drift behavior and better present actual drift values. The model results were obtained considering the mean solar flux conditions (F10.7 = 73.7 SFU) and mean altitude (~650 km) of the C/NOFS measurements. We also used the averaged values Rz12 = 10.1 and IG12 = 3.5 when running IRI. These are average values for the same period of the observations. The presentation in Figure 3b is an extension to a higher altitude of the EZDrifts results shown in Figure 2.

Fejer et al. (2013) investigated the longitudinal variation of the zonal plasma drifts with emphasis on the detection of signatures of wavenumber-4 structures (Sagawa et al., 2005; Immel et al., 2006; Hagan et al., 2007; Kil et al., 2007). For instance, the results of Fejer et al. (2013) reproduced in Figure 3a show a wavenumber-4 structure during equinox in the afternoon hours (~1400 LT) with westward peaks around 30°, 120°, 220°, and 300°. In addition to wavenumber-4 variations during the equinox, however, they also pointed out the occurrence of a longitudinal variation of the equatorial zonal drifts in the American sector during solstices.

The results in Figures 2 and 3b that EZDrifts is not capable of reproducing features such as those associated with wavenumber-4 structures and smaller (a few 10s of degrees in longitude). This is likely a result of the climatological models (IRI, HWM, MSIS) used as drivers of EZDrifts. These models are representations of parameters averaged over a wide range of longitudes, days, and/or solar flux conditions. EZDrifts, however, is capable of reproducing some of the first-order (larger scale) variations that seem to exist in the C/NOFS observations.

Figure 3 allows for a side-by-side comparison between EZDrifts and C/NOFS measurements. It shows that EZDrifts can reproduce some of the main features in the observed zonal drifts.

A comparison of Figure 3a and b shows a good agreement between the overall behavior of the reversal times predicted by EZDrifts and C/NOFS observations during June and December solstices. EZDrifts can reproduce the early reversal of the morning drifts and late reversal of the afternoon drifts during the December solstice around  $180^{\circ} - 330^{\circ}$  E longitude. Additionally, EZDrifts can also reproduce the late reversal of the morning drifts and early reversal of the afternoon drifts during June Solstice in the  $180^{\circ} - 330^{\circ}$  E longitude sector. Also, similar to the observations, EZDrifts does not show any significant longitudinal variations in the reversal times of the zonal drifts during the equinox.

We must point out that while the overall behavior of the drift reversals is reproduced by EZDrifts, some differences in the exact reversal times shown by the measurements and model can be observed. More specifically, the model seems to predict the afternoon reversals to occur later than what is seen in the C/NOFS measurements. SR21 also found this difference when comparing their model with Jicamarca ISR measurements. The differences are most likely caused by inadequacies in the driving models and should be taken into consideration when using EZDrifts.

With respect to the magnitude of the drifts, EZDrifts does show substantial longitudinal variations, particularly in the solstices during nighttime hours. EZDrifts shows weakened drifts during the December solstice and enhanced drifts during the June solstice in the  $180^{\circ} - 330^{\circ}$  E longitude sector. EZDrifts predicts much smaller longitudinal variations during Equinox.

These variations are difficult to identify in the C/NOFS observations. The measurements do not reveal the same behavior and level of longitudinal variations in the magnitude of the drifts during the Equinox and December solstice. For instance, EZDrifts does not show the enhanced westward daytime drifts around the 180° – 330° E sector observed by C/NOFS. EZDrifts does show, however, increased drifts in the 180° – 330° E sector during June solstice conditions that were detected by C/NOFS. Another interesting feature in the measurements that are not reproduced by EZDrifts is the weakening of the drifts noticeable around 0800 LT in most longitudes and all seasons but more clearly in Equinox and December solstice.

For completeness, we must point out limitations and constraints in the observations. For instance, C/NOFS was flying in an elliptical ( $401 \times 867$  km), low inclination ( $13^{\circ}$ ) orbit and, therefore, the averages in Figure 3a are a convolution of measurements distributed unevenly over a wide range of heights, longitudes, and a finite range of magnetic latitudes. One must take into consideration these observational limitations when comparing model outputs and the C/NOFS results.

Additionally, some of the differences between model results and observations, at least for nighttime conditions, can be related to ESF development and its impact on satellite observations. ESF is known to occur predominantly during Equinox and in December Solstice. Fejer et al. (2013) noted that C/NOFS observations were impacted by the occurrence of ESF irregularities. The occurrence of F-region irregularities would bias the observations to non-ESF days, regions, and altitudes. This would explain the good agreement between EZDrifts and observations during the June solstice. June solstice is a period when irregularities are less likely to occur and reach high altitudes (Gentile et al., 2006; Kil et al., 2009).

# 3.4 On the source of the longitudinal variations in the zonal drifts

We now look at the sources of the longitudinal variation of the zonal drifts predicted by EZDrifts. More specifically, we evaluate and present the contributions of the different terms on the right-hand side of equation (5) to the zonal drifts output by EZDrifts. We remind the reader that, like in previous studies (Eccles, 1998; Chau & Woodman, 2004; Rodrigues et al., 2012; Hui & Fejer, 2015; Richmond et al., 2015; Shidler & Rodrigues, 2021), the contribution of the last term in equation (5) (vertical

current) has been assumed to be negligible in this modeling effort.

Figure 4 shows the contributions of the different terms to the total zonal drifts output by EZDrifts. The top row reproduces the EZDrifts results shown in Figure 3b. Each column represents a season. The lower panels show the contribution of each term to the total zonal drifts. The first point highlighted by the results in Figure 4 is that the longitudinal variation of the zonal drifts is controlled mostly by zonal winds weighted by the Pedersen conductivity  $(U_{\phi}^P)$  term. The longitudinal variations in the total zonal plasma drifts follow closely the variation of  $U_{\phi}^P$ . Another important point illustrated by the results in Figure 4 is that the integrated meridional wind term  $\left(\frac{\Sigma_H}{\Sigma_P}U_L^H\right)$  also shows longitudinal variations, particularly during June and December solstice. The magnitude of  $U_{\phi}^P$ , however, dominates over the other two terms. More importantly, the results in Figure 4 show longitudinal variations occurring in the same longitude sector, that is, from about  $180^{\circ}$  E  $-330^{\circ}$  E.

The results in Figure 4 also show that the afternoon reversal times are mostly controlled by  $U_\phi^P$ . Therefore, differences in the model reversal times with respect to C/NOFS measurements pointed out in the previous section are most likely caused by inadequacies in the specification of winds and/or conductivities in the afternoon and evening sectors. Results of SR21 show that all three HWM wind models tend to produce reversal times that are late with respect to observations made by the Jicamarca ISR at low and high solar flux conditions.

# 3.5 On the role of the geomagnetic field in longitudinal variations of zonal drifts

The changes in the equatorial zonal drifts observed between about 180° E and 330° E suggest a relationship with the Earth's magnetic field. The location of the geomagnetic equator with respect to the geographic equator and the magnetic declination varies significantly in the same longitude sector where the changes in the zonal drifts are observed.

Since we found that  $U_{\phi}^{P}$  is the main driver of the morphology of the zonal drifts, we investigated the global behavior of the neutral winds. Figure 5 shows the zonal component of the thermospheric neutral winds predicted by HMW14 at four different altitudes as a function of latitude and longitude for 20:00 LT. Here, we point out that, at night, we expect Pedersen conductivities at F-region heights to control  $U_{\phi}^{P}$  and the wind dynamo to be representative of the F-region winds. Each season is represented per row. Again, the calculations are for the same geomagnetically quiet conditions used in the computations of the drifts shown in Figures 2–4.

Figure 5 shows that for the longitude sector between about  $0^{\circ}$  E and  $180^{\circ}$  E, the geomagnetic equator is located around the same geographic latitude (~8° N). Between about  $180^{\circ}$  E and  $330^{\circ}$  E, however, the location of the geomagnetic equator varies significantly in latitude, from ~8° N to ~10° S. The magnetic declination also changes dramatically in that longitude sector. Therefore, zonal drifts in the  $0^{\circ}$  E  $-180^{\circ}$  E sector would be dictated mostly by the wind dynamo acting on magnetic field lines around  $8^{\circ}$  N latitude. HWM14 only shows small longitudinal variations in the winds for that sector. Zonal drifts in the  $180^{\circ}$  E  $-330^{\circ}$  E sector, however, would be controlled by a wind dynamo with contributions from latitudes that vary with

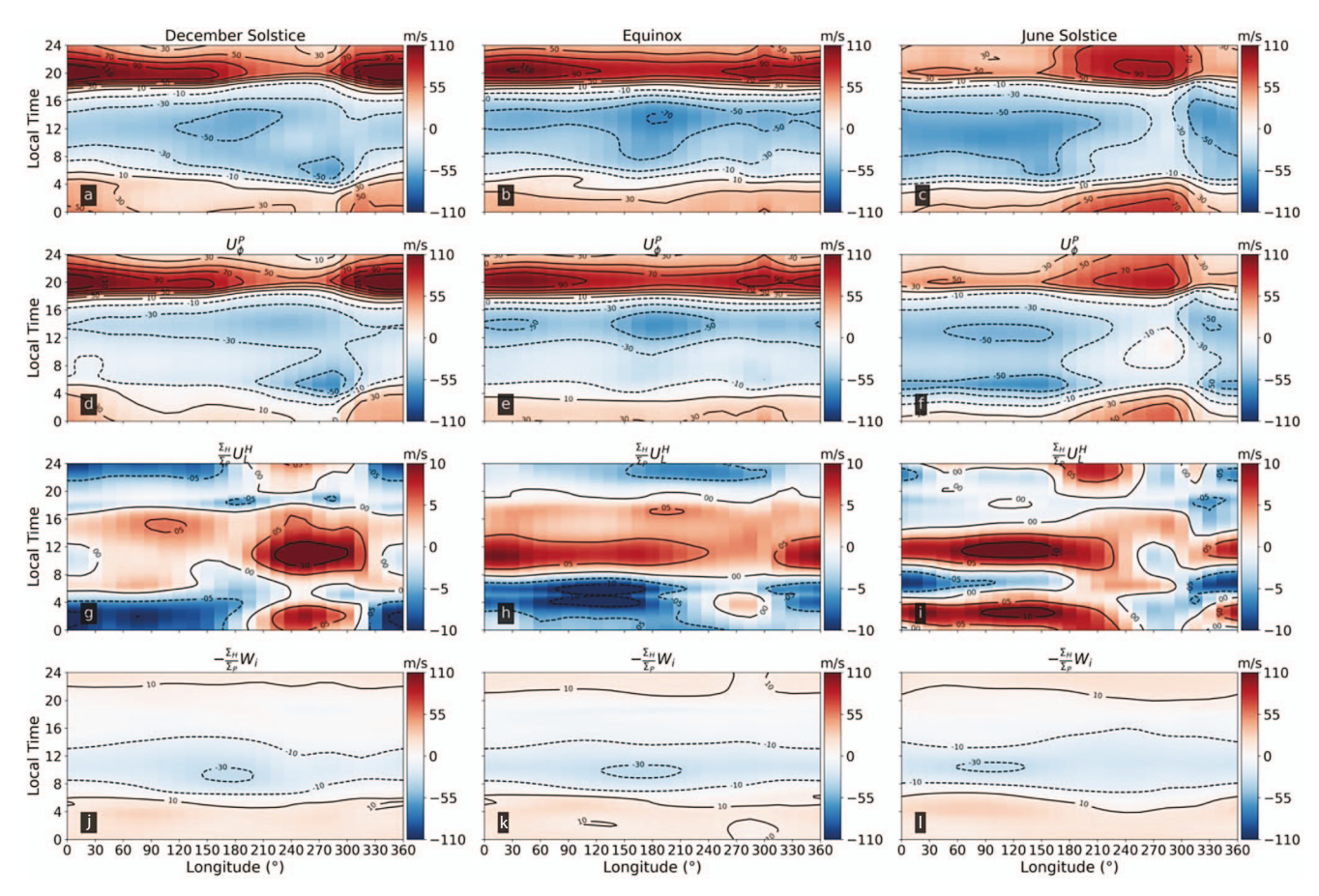


**Fig. 4.** The top row shows equatorial zonal plasma drifts at 650 km for low solar flux conditions. Each column corresponds to a season. These are the same drifts shown in Figure 3b. Contributions from each term (Eq. (5)) are shown in each row below the top panels.

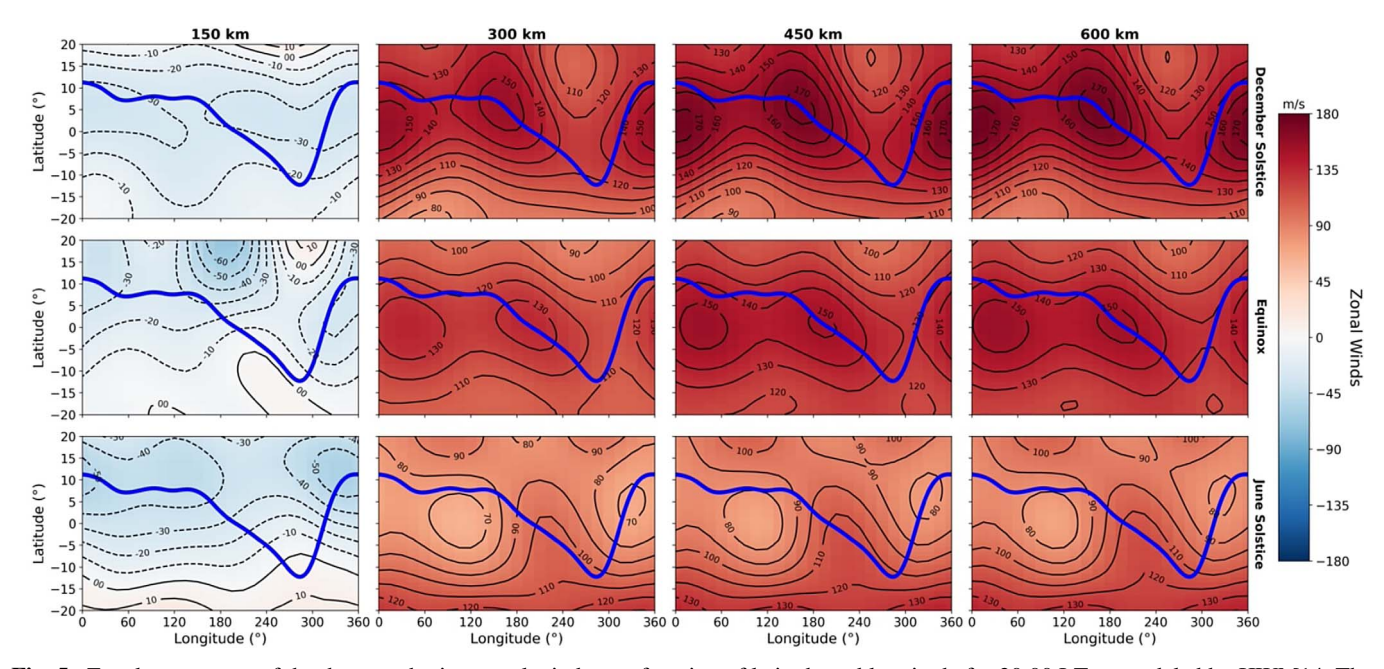


**Fig. 5.** Zonal component of the thermospheric neutral winds as a function of latitude and longitude for 20:00 LT as modeled by HWM14. The winds are the same used by EZDrifts to produce the equatorial zonal drifts shown in Figures 2–4. Each panel represents one altitude and season. The altitudes are indicated on the top of each column of panels. The seasons are indicated on the right-hand side of each row of panels. The solid blue line indicates the location of the geomagnetic equator.

longitude. This longitudinal change in the wind dynamo would produce longitudinal changes in the zonal drifts.

For instance, looking at Figure 5 (top panels) one can see that the geomagnetic equator in the  $180^{\circ} E - 330^{\circ} E$  sector is located in a region of decreased eastward winds during the December solstice. This decrease is caused by both latitudinal and longitudinal variations in the winds predicted by HWM14 for that sector. The decrease in zonal winds causes a decrease in the wind dynamo  $(\boldsymbol{U}_{\boldsymbol{\phi}}^{\boldsymbol{P}})$  and, consequently, in the magnitude of the zonal drifts for that sector (see Fig. 4a). Figure 5 (bottom panels) also shows that during the June solstice, however, the magnetic equator in the 180° E - 330° E sector is located in a region of enhanced eastward winds. The enhancement of the zonal winds causes the enhancement of the zonal plasma drifts in that longitude sector (see Fig. 4c). Finally, Figure 5 (middle panels) shows only weak latitudinal and longitudinal variations in the magnitude of the eastward winds near the magnetic equator for Equinox conditions. As a result, the wind dynamo and zonal drifts do not vary much with longitude (see Fig. 4b).

## 4 Conclusions

We described a new global climatological model of the equatorial ionospheric F-region zonal drifts (EZDrifts). The model is distributed to the community through a public repository and can be used in applications requiring an estimate of the overall behavior of the equatorial zonal drifts.

EZDrifts uses the analytic description of the zonal plasma drifts presented by Haerendel et al. (1992) and is driven by climatological models of the ionosphere and thermosphere (IRI, HWM, and MSIS) under a realistic geomagnetic field configuration provided by the IGRF model. This global model is an expansion of the climatological model of the zonal drifts first presented by Shidler & Rodrigues (2021). Their model, however, was driven by averaged height-dependent vertical drifts that were only available for three seasons and two solar flux conditions and only valid for the Peruvian (Jicamarca) longitude sector. EZDrifts replaces the average drifts used by the SR21 model (Shidler & Rodrigues, 2021) with height-independent vertical equatorial plasma drifts from the Scherliess & Fejer (1999) model which allows it to provide zonal drifts for any longitude sector and solar flux condition.

We showed that EZDrifts can reproduce the main results of the SR21 model for the Peruvian sector. Differences in the zonal drifts between EZDrifts and SR21 are mostly around 2 m/s and rarely exceed 4 m/s. More importantly, we show that EZDrifts predicts some large-scale longitudinal variations in the zonal drifts that are in good agreement with observations. More specifically, we showed that EZDrifts predicts longitudinal variations in the reversal times of the drifts that have also been detected in the observations made by the C/NOFS satellite. EZDrifts also predicts longitudinal variations in the magnitude of the drifts that are in good agreement with observations made by C/NOFS during the June solstice. Differences between the model and observations have also been identified for Equinox and December solstice conditions. The differences between the model and observations could be, at least in part, due to limitations in the measurements which were made over a wide range of altitudes, longitudes, and finite range of magnetic latitudes. The differences, especially during nighttime, could also be due to observational constraints caused by ESF. ESF occurs frequently in Equinox and December solstice and affects the ability of sensors to make adequate observations of the background plasma. Data-model comparisons also show differences in the time of the zonal plasma drift reversals in the afternoon. The model tends to predict reversals in the afternoon occurring later than what measurements show. The model reversal times are mostly controlled by the wind dynamo. Further analyses are needed to better understand the differences between the model and observations that were found in this presentation of EZDrifts. These analyses are beyond the scope of this presentation and will be carried out in a future study.

Finally, we showed the role of the geomagnetic field in creating longitudinal variations in the zonal plasma drifts. We showed that the longitudinal variations in the magnitude of the zonal plasma drifts are driven by longitudinal variations in the latitude of the magnetic equator which cause longitudinal variations in the driving wind dynamo.

# Data availability statement

A copy of the EZDrifts model used in this study is available for download at [https://doi.org/10.5281/zenodo.7685101].

Acknowledgements. The work at UT Dallas was supported by NSF awards AGS-1554926 and AGS-1916055. The editor thanks two anonymous reviewers for their assistance in evaluating this paper.

# References

Alken P, Maus S, Richmond AD, Maute A. 2011. The ionospheric gravity and diamagnetic current systems. *J Geophys Res* **116(A12)**: A12316. https://doi.org/10.1029/2011JA017126.

Bilitza D, Altadill D, Truhlik V, Shubin V, Galkin I, Reinisch B, Huang X. 2017. International Reference Ionosphere 2016: From ionospheric climate to real-time weather predictions. *Space Weather* 15(2): 418–429. https://doi.org/10.1002/2016SW001593.

Bilitza D. 2018. IRI the International Standard for the Ionosphere. *Adv Radio Sci* **16**: 1–11. https://doi.org/10.5194/ars-16-1-2018.

Chapagain NP, Fisher DJ, Meriwether JW, Chau JL, Makela JJ. 2013. Comparison of zonal neutral winds with equatorial plasma bubble and plasma drift velocities. *J Geophys Res: Space Phys* **118(4)**: 1802–1812. https://doi.org/10.1002/jgra.50238.

Chau JL, Woodman RF. 2004. Daytime vertical and zonal velocities from 150-km echoes: Their relevance to F-region dynamics. *Geophys Res Lett* **31(17)**: 17801. https://doi.org/10.1029/2004GL020800.

Coley WR, Heelis RA. 1989. Low-latitude zonal and vertical ion drifts seen by DE-2. *J Geophys Res* **94(A6)**: 6751–6761. https://doi.org/10.1029/JA094iA06p06751.

Drob DP, Emmert JT, Crowley G, Picone JM, Shepherd GG, et al. 2008. An empirical model of the Earth's horizontal wind fields: HWM07. *J Geophys Res* **113(A12)**: A12304. https://doi.org/10.1029/2008JA013668.

Drob DP, Emmert JT, Meriwether JW, Makela JJ, Doornbos E, et al. 2015. An update to the Horizontal Wind Model (HWM): The quiet time thermosphere. *Earth Space Sci* **2**(7): 301–319. https://doi.org/10.1002/2014EA000089.

- Eccles JV. 1998. A simple model of low-latitude electric fields. *J Geophys Res* **103**(A11): 26699–26708. https://doi.org/10.1029/98JA02657.
- Eccles JV, Maynard N, Wilson G. 1999. Study of the evening plasma drift vortex in the low latitude ionosphere using San Marco electric field measurements. *J Geophys Res* **104(A12)**: 28133–28143. https://doi.org/10.1029/1999JA900373.
- Eccles JV. 2004. The effect of gravity and pressure in the electrodynamics of the low-latitude ionosphere. *J Geophys Res* **109(A5)**: A05304. https://doi.org/10.1029/2003JA010023.
- Eccles JV, St. Maurice JP, Schunk RW. 2015. Mechanisms underlying the prereversal enhancement of the vertical plasma drift in the low-latitude ionosphere. *J Geophys Res* **120(6)**: 4950–4970. https://doi.org/10.1002/2014JA020664.
- Fejer BG, Scherliess L, de Paula ER. 1999. Effects of the vertical plasma drift velocity on the generation and evolution of equatorial spread F. J Geophys Res 104(A9): 19859–19869. https://doi.org/ 10.1029/1999JA900271.
- Fejer BG, de Souza J, Santos AS, Costa Pereira AE. 2005. Climatology of F region zonal plasma drifts over Jicamarca. *J Geophys Res* **110(A12)**: A12310. https://doi.org/10.1029/2005JA011324.
- Fejer BG, Tracy BD, Pfaff RF. 2013. Equatorial zonal plasma drifts measured by the C/NOFS satellite during the 2008–2011 solar minimum. *J Geophys Res: Space Phys* **118(6)**: 3891–3897. https://doi.org/10.1002/jgra.50382.
- Gentile LC, Burke WJ, Rich FJ. 2006. A climatology of equatorial plasma bubbles from DMSP 1989–2004. *Radio Sci* **41(5)**: RS5S21. https://doi.org/10.1029/2005RS003340.
- Haerendel G, Eccles JV, Çakir S. 1992. Theory for modeling the equatorial evening ionosphere and the origin of the shear in the horizontal plasma flow. *J Geophys Res* **97(A2)**: 1209–1223. https://doi.org/10.1029/91JA02226.
- Hagan ME, Maute A, Roble RG, Richmond AD, Immel TJ, England SL. 2007. Connections between deep tropical clouds and the Earth's ionosphere. *Geophys Res Lett* 34(20): L20109. https://doi.org/10.1029/2007GL030142.
- Hedin AE, Fleming EL, Manson AH, Schmidlin FJ, Avery SK, et al. 1996. Empirical wind model for the upper, middle and lower atmosphere. J Atmos Terr Phys 58(13): 1421–1447. https://doi. org/10.1016/0021-9169(95)00122-0.
- Hui D, Fejer BG. 2015. Daytime plasma drifts in the equatorial lower ionosphere. J Geophys Res 120(11): 9738–9747. https://doi.org/ 10.1002/2015JA021838.
- Hysell DL, Kudeki E. 2004. Collisional shear instability in the equatorial F region ionosphere. *J Geophys Res* **109**(**A11**): A11301. https://doi.org/10.1029/2004JA010636.
- Immel TJ, Sagawa E, England SL, Henderson SB, Hagan ME, Mende SB, Frey HU, Swenson CM, Paxton LJ. 2006. Control of equatorial ionospheric morphology by atmospheric tides. *Geophys Res Lett* 33(15): L15108. https://doi.org/10.1029/ 2006GL026161.
- Kil H, Oh SJ, Kelley MC, Paxton LJ, England SL, Talaat E, Min KW, Su SY. 2007. Longitudinal structure of the vertical E × B drift and ion density seen from ROCSAT-1. *Geophys Res Lett* **34(14)**: L14110. https://doi.org/10.1029/2007GL030018.
- Kil H, Paxton LJ, Oh SJ. 2009. Global bubble distribution seen from ROCSAT-1 and its association with the evening prereversal enhancement. *J Geophys Res* **114(A6)**: A06307. https://doi.org/10.1029/2008JA013672.
- Klobuchar JA, Anderson DN, Doherty PH. 1991. Model studies of the latitudinal extent of the equatorial anomaly during equinoctial conditions. *Radio Sci* 26(4): 1025–1047. https://doi.org/10.1029/ 91RS00799.

- Kudeki E, Bhattacharyya S. 1999. Postsunset vortex in equatorial Fb region plasma drifts and implications for bottomside spread-F. J Geophys Res 104(A12): 28163–28170. https://doi.org/10.1029/1998IA900111
- Kudeki E, Akgiray A, Milla M, Chau JL, Hysell DL. 2007. Equatorial spread-F initiation: Post-sunset vortex, thermospheric winds, gravity waves. *J Atmos Solar-Terr Phys* **69**(**17–18**): 2416–2427. https://doi.org/10.1016/j.jastp.2007.04.012.
- Liu J, Liu H, Wang W, Burns AG, Wu Q, et al. 2018. First results from the ionospheric extension of WACCM-X during the deep solar minimum year of 2008. *J Geophys Res: Space Phys* **123**(2): 1534–1553. https://doi.org/10.1002/2017JA025010.
- Picone JM, Hedin AE, Drob DP, Aikin AC. 2002. NRLMSISE-00 empirical model of the atmosphere: Statistical comparisons and scientific issues. *J Geophys Res: Space Phys* **107**(**A12**): SIA 15. https://doi.org/10.1029/2002JA009430.
- Richmond AD, Fang TW, Maute A. 2015. Electrodynamics of the equatorial evening ionosphere: 1. Importance of winds in different regions. *J Geophys Res* **120(3)**: 2118–2132. https://doi.org/10.1002/2014JA020934.
- Rodrigues FS, Crowley G, Heelis RA, Maute A, Reynolds A. 2012. On TIE-GCM simulation of the evening equatorial plasma vortex. *J Geophys Res* **117(A5)**: A05307. https://doi.org/10.1029/2011JA017369.
- Rodrigues FS, Shume EB, de Paula ER, Milla M. 2013. Equatorial 150 km echoes and daytime F region vertical plasma drifts in the Brazilian longitude sector. *Ann Geophys* **31(10)**: 1867–1876. https://doi.org/10.5194/angeo-31-1867-2013.
- Sagawa E, Immel TJ, Frey HU, Mende SB. 2005. Longitudinal structure of the equatorial anomaly in the nighttime ionosphere observed by IMAGE/FUV. *J Geophys Res* **110(A11)**: A11302. https://doi.org/10.1029/2004JA010848.
- Scherliess L, Fejer BG. 1999. Radar and satellite global equatorial *F* region vertical drift model. *J Geophys Res* **104(A4)**: 6829–6842. https://doi.org/10.1029/1999JA900025.
- Shidler SA, Rodrigues FS. 2019. On the magnitude and variability of height gradients in the equatorial F region vertical plasma drifts. *J Geophys Res: Space Phys* **124(6)**: 4916–4925. https://doi.org/10.1029/2019JA026661.
- Shidler SA, Rodrigues F, Fejer BG, Milla M. 2019. Radar studies of height-dependent equatorial F region vertical and zonal plasma drifts. *J Geophys Res: Space Phys* **124(3)**: 2058–2071. https://doi.org/10.1029/2019JA026476.
- Shidler SA, Rodrigues FS. 2021. On a simple, data-aided analytic description of the morphology of equatorial F-region zonal plasma drifts. *Prog Earth Planet Sci* **8**: 26. https://doi.org/10.1186/s40645-021-00417-8.
- Shidler SA, Rodrigues FS. 2022. An electrodynamics model for data interpretation and numerical analysis of ionospheric missions and observations (DINAMO). *Prog Earth Planet Sci* **9**: 7. https://doi.org/10.1186/s40645-021-00462-3.
- Smith JM, Rodrigues FS, Fejer BG, Milla MA. 2016. Coherent and incoherent scatter radar study of the climatology and day-to-day variability of mean F region vertical drifts and equatorial spread F. *J Geophys Res: Space Phys* **121(2)**: 1466–1482. https://doi.org/10.1002/2015JA021934.
- Smith JM, Klenzing J. 2022. Growin: Modeling ionospheric instability growth rates. *J Space Weather Space Clim* **12**: 26. https://doi.org/10.1051/swsc/2022021.
- Stoneback RA, Heelis RA, Burrell AG, Coley WR, Fejer BG, Pacheco E. 2011. Observations of quiet time vertical ion drift in the equatorial ionosphere during the solar minimum period of 2009. *J Geophys Res* **116(A12)**: A12327. https://doi.org/10.1029/2011JA016712.

Thébault E, Finlay CC, Beggan CD, Alken P, Aubert J, et al. 2015. International geomagnetic reference field: The 12th generation. *Earth Planets Space* **67**: 1–19. https://doi.org/10.1186/s40623-015-0228-9.

Zhan W, Rodrigues FS. 2018. June solstice equatorial spread F in the American sector: A numerical assessment of linear stability aided by incoherent scatter radar measurements. *J Geophys Res: Space Phys* **123**(1): 755–767. https://doi.org/10.1002/2017JA024969.

**Cite this article as**: Massoud AA, Shidler SA & Rodrigues FS 2023. A height-dependent climatological model of the equatorial ionospheric zonal plasma drifts (EZDrifts): Description and application to an analysis of the longitudinal variations of the zonal drifts. *J. Space Weather Space Clim.* **13**, 8. https://doi.org/10.1051/swsc/2023006.